

A New Spike Detection Algorithm for Extracellular Neural Recordings

Shahjahan Shahid*, Jacqueline Walker, *Member, IEEE*, and Leslie S. Smith, *Senior Member, IEEE*

Abstract—Signals from extracellular electrodes in neural systems record voltages resulting from activity in many neurons. Detecting action potentials (spikes) in a small number of specific (target) neurons is difficult because many neurons, both near and more distant, contribute to the signal at the electrode. We consider some nearby neurons as target neurons (providing a signal) and all the other contributions to the signal as noise. A new algorithm for spike detection has been developed: this applies a cepstrum of bispectrum (CoB) estimated inverse filter to provide blind equalization. This technique is based on higher order statistics, and seeks to find a sequence of event times or delta sequence. We show that the CoB-based technique can achieve a 98% hit rate on an extracellular signal containing three spike trains at up to 0 dB SNR. Threshold setting for this technique is discussed, and we show the application of the technique to some real signals. We compare performance with four established techniques and report that the CoB-based algorithm performs best.

Index Terms—Action potential, cepstrum of bispectrum (CoB), extracellular recording, higher order statistics (HOS), inverse filtering, spike detection.

I. INTRODUCTION

THE IDENTIFICATION of spikes (action potentials) in an extracellular recording is a difficult problem as a large number of neural signals contribute to the recorded signal. Automated spike detection, the subject of this paper, is normally followed by spike sorting, so that spike detection is critically important if spike sorting is to work properly. Since it is often not possible to precisely place extracellular electrodes to isolate a single neuron, the microelectrode tip is surrounded by many neurons, and therefore, detects many neurons' electrical activities. The closest neurons result in the highest electrical activity at the tip, but surrounding neurons superimpose activity changes on the amplitude and shape of the signal. In addition, signal transfer from neuron to electrode may be resistive and/or capacitive, resulting in weak signals whose shape and amplitude differ from intracellular spikes because of the transfer path characteristics [1], [2]. Perhaps, most importantly, the activity of

distant neurons may appear as noise, which is highly correlated with the target signal [3]. Other difficulties with extracellular recording are that the shapes and amplitudes of the signal of interest are influenced by many factors: most notably, the cell geometry, the distribution and density of ion channels, and the position of the recording electrode with respect to electrically active membranes [4]. Altogether, extracellular spike recordings are inevitably corrupted by noise from varied sources: the recording hardware, the ambient recording environment, and the spatially averaged activity of distant cells [5]. All these issues make the problem of spike detection challenging.

The simplest and most widely used technique for spike detection is amplitude thresholding that relies on the signal amplitude without any preprocessing beyond high-pass filtering [6]. This technique searches for an event that crosses user-specified amplitude thresholds [7], which can be set manually from visual inspection or automatically (e.g., as the mean or median plus or minus a multiple of the estimated standard deviation of the signal [3]). Although it is easy to implement in hardware [8] and attractive for real-time implementation because of its computational simplicity, the performance of these techniques deteriorate rapidly at low SNR ratio [9]. For consideration of different shaped spikes from different neurons, a windowed discriminator technique has been proposed in [10]. This technique first uses a positive-going crossing of a threshold to find the start of the time window. The duration of the window is preset (0.9 ms in [10]; we found the performance to be better by using 3 ms for real signals). A spike event is detected only if the low-pass-filtered signal crosses a negative threshold level within this time window. The main drawback of either of the threshold methods is that overlapping neural spikes are normally considered as a single spike. This results in a reduction of the efficacy of the thresholding technique [11]. To overcome this, Chandra and Optican [3] and Atiya [12] proposed the use of artificial neural networks to discriminate overlapping spikes.

The instantaneous energy of an extracellular signal has been used to highlight the spike peak by computing the energy difference between the signal's current power and the power in adjacent time intervals [13]. A related approach computes a nonlinear energy operator (NEO) by utilizing the product of the instantaneous amplitude and frequency of the extracellular signal, which enhances the spike event [14], [15]. Both methods use signal amplitude in their energy computation without employing any noise management technique, and therefore, do not perform well on noisy signals. Other spike detection methods, largely ignoring the presence of noise in the signal, utilize the first derivative of the signal [16], [17] or the signal's structure for designing morphological filters [18].

Manuscript received September 5, 2008; revised December 23, 2008, March 31, 2009, and May 29, 2009. First published July 17, 2009; current version published March 24, 2010. This work was supported by the U.K. Engineering and Physical Sciences Research Council under Grant EP/E002331/1 (Code analysis, repository and modeling for e-Neuroscience). *Asterisk indicates corresponding author.*

*S. Shahid was with the Department Computing and Mathematics, University of Stirling, Stirling, Fk9 4LA, U.K. He is now with the University of Ulster, Coleraine, BT52 1SA, U.K. (e-mail: ssh@cs.stir.ac.uk).

J. Walker is with the Department of Electronic and Computer Engineering, University of Limerick, Limerick, Ireland.

L. S. Smith is with the Department Computing and Mathematics, University of Stirling, Stirling, Fk9 4LA, U.K.

Digital Object Identifier 10.1109/TBME.2009.2026734

A different technique is template matching, originating from image processing [19]. In this approach, templates that represent a typical waveform are used as a standard. The first stage of this technique is to pick as template a waveform that represents a typical spike shape. Second, the algorithm locates possible events in the signal that “closely resemble” the template, and finally, there is a thresholding stage. Early techniques often started with the experimenter identifying some good spikes, and using them to train a filter [20]. However, this is impractical where there are large numbers of electrodes; this paper, therefore, deals with automated spike detection. For automatic template selection, the method requires amplitude or duration bootstrapping to generate approximations of actual spikes [21]. There are many available methods for determining similarity of sections of a signal, such as sum-of-squared differences [22], convolution [23], cross correlation [24], and maximum likelihood [25]. The template matching algorithm often distinguishes spike events better than simple threshold algorithms. But this improved performance relies on *a priori* knowledge of the spike shape to form the template. The performance again decreases in low SNR, since the automatic selection of a template in a noisy signal is very difficult. In addition, overlapping spikes produce a novel shape of spike that may worsen the performance of this technique.

Transformation and decomposition of signals are very common procedures in signal processing. Spike features may be observed in the Haar-transformed domain [26], which is a form of wavelet transform. The wavelet transform carries out a correlation function with the mother wavelet, and therefore, given a good choice of mother wavelet, the spike properties are enhanced in the coefficients of the continuous-wavelet transform [4], [27] and also in the discrete-wavelet transform [28], [29]. The major attraction of wavelets is their ability to separate signals from noise by thresholding the wavelet coefficients, and hence, this technique performs well even in poor SNR [9]. The main drawback of this technique is the assumption of a single spike shape resulting in wavelet choice that is suboptimal for other spikes.

In this paper, we propose a new spike detection algorithm that only utilizes the cepstrum of bispectrum (CoB) [30] as part of an inverse filtering technique. This technique was originally published in [31], but this paper considerably extends these initial results. Since the CoB is a higher order statistic (HOS) and because of the inherent properties of HOSs, any estimates from it are free from the effect of Gaussian background noise, although they may still be subject to noise resulting from the variance due to data truncation. In addition, as the CoB has a firm foundation in the theory of system estimation, our approach can estimate spikes even from overlapping signals. The algorithm is fully automatic and does not require any prior information about spike shape, or maximum or minimum spike rate.

Section II describes the algorithm in detail. We assessed our approach on two types of data: synthetic signals (as proposed in [1]), reported in Section III, and real data from Buzsaki’s laboratory [32], reported in Section V. Our technique proves useful when there are multiple spike trains in a single extracellular signal. We compare our algorithm with some established

algorithms utilizing plain thresholding, energy, morphology, and wavelet techniques.

II. NEW SPIKE DETECTION ALGORITHM

The new algorithm was originally developed for a simple neurophysiological signal model in which there is one target neuron. Partly because of the adaptiveness of this algorithm, and partly because it works in the frequency domain, it also works well on multiple-neuron extracellular signals. The key steps of the new spike detection algorithm are: 1) estimate an appropriate inverse filter from the original signal; 2) perform deconvolution using the estimated inverse filter; and 3) suppress the noise, and then threshold the deconvolved signal. To describe the spike detection algorithm in detail, we start from a simple neurophysiological model.

A. Simple Neurophysiological Model

A single-channel neurophysiological signal can be modeled as the output of a filtered point process. The signal also contains some other filtered point process data, which are called noise. Mathematically, an observed single-channel neurophysiological signal $x(t)$ is assumed to be the output of a linear time invariant (LTI) system that can be expressed as

$$x(t) = e(t) \otimes s(t) + w(t) \quad (1)$$

where t is the time index, $e(t)$ is the input point process, $s(t)$ is the filter of the process (also known as the transfer function), and $w(t)$ is the noise that may contain both correlated signals with different amplitudes, as well as uncorrelated signals. It is strictly assumed that the input process $e(t)$ is a Poisson process that is non-Gaussian in nature over a long period. From a neurophysiological viewpoint, $s(t)$ is the filter built up from the intracellular spike shape and the spike transfer characteristic, integrated over the spiking surface of the neuron, and $e(t)$ is the sequence of events (considered as a delta impulse sequence).

B. Design of Spike Detection Algorithm

Blind deconvolution theory describes many techniques for recovering the system filter ($s(t)$) from an unknown LTI system output signal ($x(t)$). Inverse filtering is one solution for estimating the input signal from the filter’s output signal.

Suppose, we have a filter (called an inverse filter) $s^{-1}(t)$, which is an inverse of $s(t)$, i.e., $s^{-1}(t) \otimes s(t) = \delta(t)$, or in the frequency domain $S^{-1}(n)S(n) = 1$ (where n is the frequency index). Now, if we apply this filter $s^{-1}(t)$ to $x(t)$ [from (1)], we get an output $z(t)$ as

$$\begin{aligned} z(t) &= x(t) \otimes s^{-1}(t) \\ &= [e(t) \otimes s(t) + w(t)] \otimes s^{-1}(t) \\ &= e(t) \otimes s(t) \otimes s^{-1}(t) + w(t) \otimes s^{-1}(t) \\ &= e(t) + e_w(t) \end{aligned} \quad (2)$$

where $e_w(t)$ is a noise component generated by the effect of the inverse filter on the noise. The inverse filter’s output $z(t)$ should be similar to an input delta sequence $e(t)$, if $e_w(t)$ is cut off or

attenuated by applying some extra processing (e.g., denoising or noise thresholding) to $z(t)$.

In the following sections, we describe a technique to estimate the inverse filter ($s^{-1}(t)$) blindly from only the considered signal $x(t)$, and a procedure to suppress and threshold noise acquired from the inverse filter output signal $z(t)$.

1) *Inverse Filter Estimation*: The time domain inverse filter $s^{-1}(t)$ of any invertible linear process can be estimated from its frequency domain function $S^{-1}(n)$. Alternatively, using the equation ($S^{-1}(n)S(n) = 1$), the inverse filter can be computed from frequency domain transfer function $S(n)$ as

$$\begin{aligned} s^{-1}(t) &= F^{-1}[S^{-1}(n)] \\ &= F^{-1}\left[\frac{1}{S(n)}\right] \quad \text{and} \quad S(n) \neq 0 \end{aligned} \quad (3)$$

where $F_1^{-1}[\bullet]$ denotes the inverse Fourier transform. Now, we use the CoB-based blind filter estimation technique to estimate the system transfer function ($S(n)$) from the signal $x(t)$. The CoB of the output of any LTI system can be computed by applying the 1-D inverse Fourier transform to the log bispectrum [33]. The bispectrum is defined as the 2-D Fourier transform of the third-order moment (see [34, p. 488]), or alternatively, as the cumulant contribution of three Fourier components [35]. The CoB is generally computed from the signal's frequency domain representation by using

$$\begin{aligned} c_{B_x}(n, t) &= F_1^{-1}[\log\{B_x(n, l)\}]_l \\ &= F_1^{-1}[\log\{X(n)X(l)X^*(n+l)\}]_l \end{aligned} \quad (4)$$

where $c_{B_x}[\bullet]$ is the CoB of the signal, $X[\bullet]$ is the frequency domain representation of $x(t)$, n and l are the frequency indexes, $F_1^{-1}[\bullet]_l$ denotes the 1-D inverse Fourier transform to be applied to the frequency axis l , and $B_x(n, l)$ is the bispectrum of $x(t)$. The CoB value is an expression in terms of cepstral time (t) and the frequency (n) plane. The CoB was expressed in [30] in terms of the filter's transfer function [as seen in (5)], and therefore, by setting the cepstral time index to 0, the log of the system filter can be recovered

$$\begin{aligned} c_{B_x}(n, t) &= F_1^{-1}[\log\{\gamma_e S(n)S(l)S^*(n+l)\}]_l \\ &= \log\{\gamma_e\}\delta(t) + \log\{S(n)\}\delta(t) + c_s(t) \\ &\quad + e^{-j2\pi km/N} c_s(-t) \end{aligned} \quad (5)$$

$$\begin{aligned} c_{B_x}(n, 0) &= \log\{S(n)\} + \log\{\gamma_e\} + c_s(0) + e^{-j2\pi km/N} c_s(0) \\ &= \log\{S(n)\} + \kappa \end{aligned} \quad (6)$$

where κ is independent of n , $c_s(t)$ is the cepstrum of the filter $s(t)$, and γ_e is the skewness of the input process $e(t)$. The skewness is the third-order moment of the process [i.e., analogous to the mean (first order) and variance (second order)]. The aforementioned expression shows that the CoB is a complex measurement that carries both the filter's Fourier magnitude and phase information. The main properties of this statistic are that it carries the logarithmic value of the frequency-domain system transfer function. As the CoB suppresses any Gaussian noise effects due to the properties of HOS, it is possible to reconstruct filter information blindly from any output signal even at a low

SNR [30]. The frequency domain filter $S(n)$ of our model neurophysiological signal $x(t)$ is computed with the relation stated in [30, eq. (12)] as

$$S(n) = \exp[c_{B_x}(n, 0) - c_{B_x}(0, 0)]. \quad (7)$$

We also use the phase unwrapping procedure in bispectrum computation, which is described in the same paper. The fast Fourier transform (FFT) algorithm is used throughout to change the data domain between time and frequency. The resolution (number of points) in the FFT must be chosen so that the frequency spectrum of the signal of interest (here, neurophysiological spikes) is well represented.

2) *Noise Suppression and Thresholding*: The noise in neurophysiological recordings is a mixture of correlated and uncorrelated neural signals whose amplitude is assumed to be lower than the signal amplitude. (In addition, there may be Gaussian noise from the instrumentation as well.) Consequently, the amplitude of the noise term at the output of the inverse filter [$e_w(t)$ of (2)] should be lower than the amplitude of the associated delta sequence (point process) of interest, ($e(t)$). In addition, the characteristics of this noise term ($e_w(t)$) are different from those of a point process ($e(t)$): one major difference is that the point process must be a delta sequence, which is rarely the case for the noise term because it is the combination of many sources that interfere with each other constructively and destructively.

If the neurophysiological recordings have a high SNR, then the point process can be found by using simple amplitude thresholding on (2). For lower SNR, amplitude thresholding alone may not work well and additional processing applied to $z(t)$ is necessary in order to enhance the delta sequence, as well as to suppress the noise term. We, therefore, denoise the inverse-filtered output signal $z(t)$ [see (2)] using the discrete-stationary-wavelet transformation employing the first coiflet wavelet (coif1) for its decomposition and reconstruction. This was chosen because the shape of each delta element in a noise free $z(t)$ is very similar to the shape of the first coiflet wavelet. Note that the delta sequence found in (2) is independent of the shape of the extracellular spike or additive noise.

We follow the standard denoising procedure described in the MATLAB user's guide [36]. The denoising procedure is implemented in two steps: the inverse filtered signal $z(t)$ is, first, decomposed to provide the first three detail and approximation coefficients from the coiflet-wavelet transform, and second, three denoised signals are reconstructed using only one level of detail coefficient with zero approximation. We choose the most highly skewed signal from the original (inverse filtered) and denoised signals. This signal, referred to as the denoised inverse-filtered signal, $d_z(t)$ shows an enhanced delta sequence with a low value for the noise term $e_w(t)$.

The amplitude of the estimated delta sequence has a theoretical maximum of 1 due to the use of subtraction in (7). But, in practice, it depends on: 1) how accurately the inverse filter is estimated and 2) how corrupted the recorded spike is. Since the extracellular signal has multiple spike trains, the algorithm estimates an average inverse filter so that the amplitude of the delta sequence may not achieve its maximum value. Similarly, greater corruption of the extracellular signal impairs the estimate of an

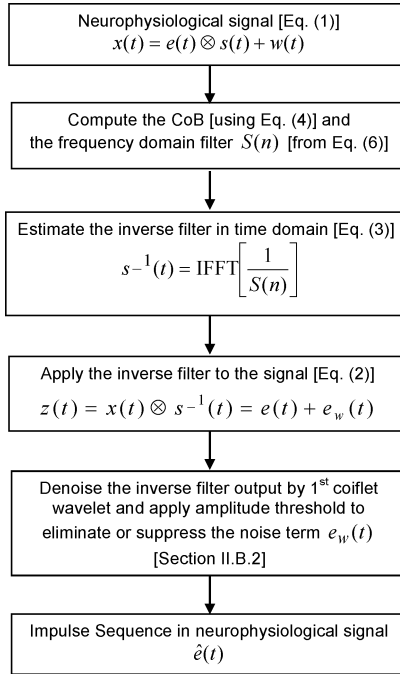


Fig. 1. Block diagram of the new spike detection algorithm. For a detailed description, see Section II.

accurate average inverse filter. Regardless of the amplitude of the delta sequence, the amplitude of the noise term of the denoised inverse-filtered signal [$e_w(t)$ of (2)] should be below that of the delta sequence, if the extracellular signal has SNR better than 0 dB. The overall effect of increasing noise is twofold: the amplitude of the delta sequence falls, and the amplitude of the noise term rises.

We, therefore, use amplitude thresholding based on the peak signal level to cut the noise term from the denoised signal. The selection of the amplitude threshold level is very sensitive: a low threshold level can increase false detection (false positive), while a higher threshold level can increase the number of missing spikes (false negative). Equation (8) is applied to cut out the noise term from the denoised inverse-filtered signal $y(t)$ (where $y(t) = d_z(t)$; $d_z(t)$ is $z(t)$ denoised using the coiflet wavelet)

$$\theta_y = ky_m(t) \quad (8)$$

where k is a constant ($0 < k \leq 1$) and $y_m(t)$ is the maximum amplitude of the signal $y(t)$. The signal above threshold value [i.e., $\hat{e}(t) = \max(0, y(t) - \theta_y)$] may now be used to estimate spike times. We use the time of occurrence of the peaks of $\hat{e}(t)$ to estimate these times.

A block diagram of the new algorithm is illustrated in Fig. 1.

C. Effectiveness of Algorithm

The extracellular electrophysiological signal is assumed to be a linear mixture of many neural spike trains, arriving through different transfer functions at the sensor, and thus, with different amplitudes and possibly shapes. Each spike train may be considered as a filtered Poisson process. However, in an extracellular recording, only a very small number of spike trains

can be detected as spiking events because the rest of the spike trains have a lower amplitude, and thus, are considered as neural noise. The spiking events come from neurons very close to the electrode: we call them the dominant spike trains. The (noise) spike trains originate from neurons further away from the detector (electrode), and as a result, have a lower amplitude at the detector: further, since the number of neurons at distance r from the electrode increases as r^2 , the number of neurons contributing to the noise is much larger. Since this neural noise is a sum of a large number of Poisson processes, the linear mixture of these processes resembles white noise (Gaussian or non-Gaussian). Some neighboring (but not dominant) neurons fire in a way correlated with the dominant neurons. These can produce relatively large signals on occasion due to a number of these neurons firing near-simultaneously. However, such signals occur infrequently, and do not resemble spike trains, and are thus classified as noise. HOS (in this case, the bispectrum) suppress the effect of any Gaussian or symmetrically distributed non-Gaussian noise, and as a result, the technique works well at suppressing noise in these neurophysiological signals.

The key task of the technique is to estimate an appropriate inverse filter from the signal for deconvolution. To compute the inverse filter, the technique estimates the frequency domain filter from the signal. Since the extracellular signal contains a number of dominant spikes, the technique estimates an average filter (in frequency domain). In the calculation of this average filter, the frequency components of all spikes (whether originating from dominant or other neurons) are included. However, the technique simply ignores the frequency components from those spikes that are subsumed into the white noise.

The time domain (average) inverse filter is calculated from the average frequency domain filter. Since the filter estimation is based on HOS (here, CoB), the estimated inverse filter is free from the effects of the neural noise. Thus, deconvolution using the average inverse filter reconstructs the delta function of the process. The estimated delta functions produced have different amplitudes depending on the spectral components of the filter of the Poisson process. This is to say, different neurons produce different sizes of estimated delta functions because the transfer function from the (putative) delta signal to the electrode is different for different neurons.

On a PC with a dual-core 2.66 GHz processor and 3.25 GB RAM, the algorithm (coded in MATLAB) takes between 6 and 8 s to process a 30-s-long single extracellular signal sampled at 20 kHz. Highly noisy signals (poorer than 0 dB SNR) can require more processing, and therefore, take longer, but always less than half of the signal duration using the aforementioned equipment.

III. RESULTS AND ANALYSIS FROM SYNTHESIZED DATA

The new spike detection algorithm is based on statistical methods, and therefore, the performance is subject to errors. The best way to validate the performance of this algorithm is to test it using Monte Carlo trials. To ensure consistent results, the number of trials needs to be sufficiently high, and the trials

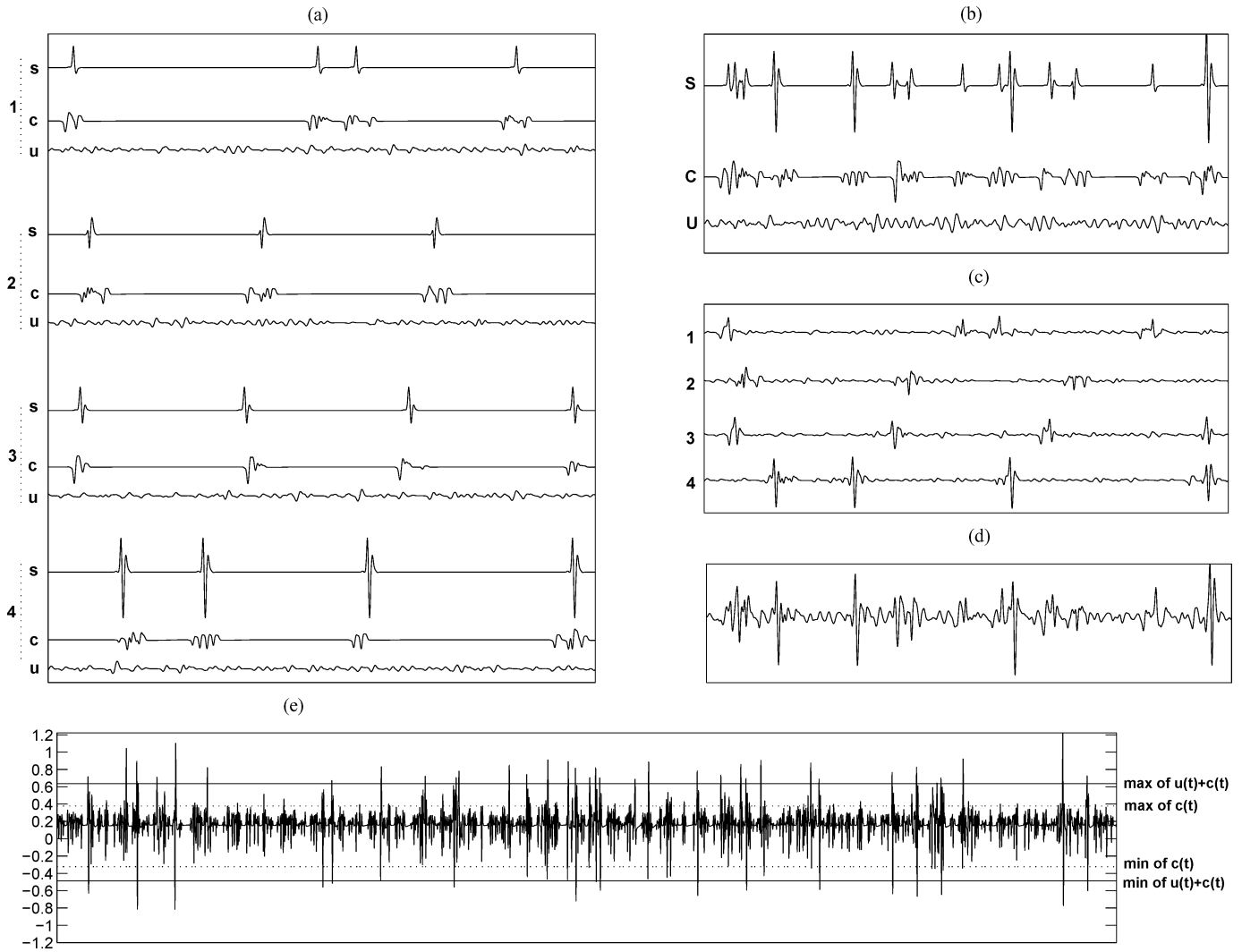


Fig. 2. Synthesized extracellular signal generation (using the algorithm from [1]). It is assumed here that the extracellular signal reflects noisy signals from four spiking neurons. (a) Contributing signal from four neurons. Each neuron provides one spike train (s) and there is neural noise from neighboring neurons, some of which are correlated (c) and some uncorrelated (u). (b) Typewise linear sum of the contributing signals, i.e., the signal S , C , and U are the sum of all s , all c , and all u , respectively. (c) Neuronwise extracellular signal, which is the linear sum of, respective, contributing signals s , c , and u , which is linear sum of all contributing neuron signals. (d) Synthesized extracellular signal, which is linear sum of all contributing neuron signals. (e) Synthesized extracellular test signal at SNR = 5 dB. This signal contains spike trains from four target neurons plus 7 correlated and 15 uncorrelated neural signal, as shown previously. The duration of this test-illustrated signal is 1 s and the spike rate of each target neuron is 10 Hz, i.e., 40 number of spikes with different amplitude are present in the illustrated test signal.

must be independent of each other. Ground-truth information is necessary for error measurement, and this is very difficult to obtain in real extracellular recordings (but see Section V). Here, we synthesize the neurophysiological signal, so that we have information on the spike train. Further, we can manipulate the number of spike trains, the spike timings, the spike shape, and the noise level.

A. Model of Synthesized Neurophysiological Signal

We use the algorithm and code from [1] for generation of independent synthesized signals. This models the extracellular signal as a linear mixture of three types of signal: spike train, neural correlated noise, and uncorrelated noise. An example of this technique is shown in Fig. 2. It shows the generation of a synthesized extracellular signal [see Fig. 2(d)], which is the

sum of four dominant spike trains [see Fig. 2(c)]. Each spike train consists of three types of signal: spike train (s), correlated noise (c), and uncorrelated noise (u), as shown in Fig. 2(a). Fig. 2(b) shows the individual sum of all s , c , and u signals from Fig. 2(a), and their linear mixture results in the final synthesized extracellular signal [see Fig. 2(d)]. The signals participating in the synthesized extracellular signal are the following.

- 1) *Spike train [signal S in Fig. 2(b)]:* It is a linear mixture of multiple-target neural spike trains where each spike train is randomly distributed (using a Poisson process, but with minimum 1 ms interspike time interval). The signal is generated by convolving a spike shape with the spike train (a different shape is used for each target neuron). The shape of the spike is a realistic extracellular spike signal generated from an intracellular signal [1]. As shown in the example (see Fig. 2), the spike events in each train

[see Fig. 2(a)] are randomly distributed. The spike shape is different for each spike train.

- 2) *Correlated neural noise [signal C in Fig. 2(b)]:* It is a linear mixture of a number of neural spike trains generated by neighboring neurons. The noise spike events are highly correlated with the target neural spikes (each spike is generated with a noisy-neuron-dependent probability within a short time interval of each spike from the neuron with which it is correlated; the probabilities vary from 0.3 to 0.8, and the time intervals vary from ± 8 to ± 12 ms); See Fig. 2(a), where the spike-like neural signal c with relatively low amplitude appears at about the same time as the target neural spike. This signal arises from neighboring neurons and is very confusing in spike detection. Actual signals are generated in the same way as the original spike train.
- 3) *Uncorrelated noise [signal U in Fig. 2(b)]:* It is a set of uncorrelated randomly distributed spike signals. These signals are generated from spikes created by a number of Poisson processes (one per uncorrelated neuron). Actual signals are generated in the same way as the original spike train.

B. Signal-to-Noise Ratio

The instantaneous (power) SNR is the ratio of signal power to background noise power at that instant. There is a range of techniques for SNR estimation. It can be computed from the ratio of the amplitude of the signal to the standard deviation of (zero mean) background noise. Alternatively, it can be computed from the rms value of the signal and the noise. These techniques are most appropriate where the signal is of near-constant amplitude. But, in neurophysiology, the signal (spike) is highly dynamic. In this case, different techniques may be used, as discussed in [1], [4], and [37].

Following [1], we computed the SNR as the ratio of the maximum peak-to-peak amplitudes of the spike signal and the background noise. (We note that using the ratio of peak spike amplitude to RMS noise would give a higher SNR.) For the signal generated by multiple neurons, different peak-to-peak amplitudes may be observed from different neural spike trains, and therefore, average peak-to-peak amplitude is used instead of single maximum peak-to-peak amplitude. In our experiment with synthesized signals, we compute an average peak-to-peak spike amplitude (\bar{S}_{pp}) from all contributing spike trains [signal s in Fig. 2(a)]. The background noise (N_{pp}) is the maximum peak-to-peak amplitude of the neural and other noise signals [signal c plus u in Fig. 2(a)]. The equation for SNR in decibels that we use is

$$\text{SNR} = 20 \log_{10} \left[\frac{\bar{S}_{pp}}{N_{pp}} \right]. \quad (9)$$

To observe the performance of an algorithm at different SNRs, we simply manipulate the amplitude of noise to provide different SNRs (as for an example, the relative amplitude ratio of $s(t)$, $u(t)$, and $c(t)$ is 1 : 0.56 : 0.56 for 5 dB, 1 : 1 : 1 for 0 dB, and 1 : 1.77 : 1.77 for -5 dB SNR).

C. Performance Quantification

The spike detection ability of the new algorithm can be determined by applying it to a number of different types of test signals whose ground truth is known. We compare the ground truth with the algorithm-detected spike events and produce a confusion matrix for each test signal. On each event comparison, we allow a tolerance of ± 0.5 ms. In addition, since the amplitude threshold used in the new algorithm (discussed in Section II-B2) is highly dependent on SNR value, we tune the threshold in each test signal so that it minimizes the sum of type I (false positive) and type II errors (false negative). The formulas used to quantify the performance of the algorithm [38] are as follows:

$$\begin{aligned} \text{Hit rate} &= \frac{N_{\text{cds}}}{N_{\text{trs}}} \times 100 & \text{Precision} &= \frac{N_{\text{cds}}}{N_{\text{ds}}} \times 100 \\ \text{False-positive rate} &= \frac{N_{\text{fds}}}{N_{\text{trns}}} \times 100 \end{aligned} \quad (10)$$

where N_{cds} is the number of correctly detected spike events (true positive), N_{trs} is the total number of true spike events in the test signal (true positive and false negative), N_{fds} is the number of falsely detected spike events (false positive), N_{trns} is the number of true nonspike events (true negative plus false positive) and N_{ds} is the number of spike events detected by the method (true positive plus false positive). Note that we assume a minimum interspike interval (ISI) of 1 ms, limiting N_{trns} to a maximum of 1000 s^{-1} .

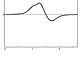
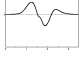
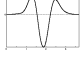
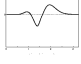
The aim of a spike detection method is to minimize N_{fds} and maximize N_{cds} . This implies maximizing the hit rate and precision at the same time, and minimizing the false-positive rate. Since we are concerned with the detection of spike events, we use hit rate and precision to observe the performance of the algorithm.

D. Performance of Algorithm on Different Test Signals

A number of test signals have been used to evaluate the new algorithm. These test signals can be categorized in different ways: 1) number of dominant spike trains with different spike shapes in the signal; 2) spike rate(s) in the signal; and 3) level of additive neural noise (correlated plus uncorrelated, i.e., SNR). In addition, we consider one or more sets of synthetic neurophysiological signals from each category: where one set of signals consists of 50 synthetic test signals each 5 s long, and sampled at 24 kHz. Our test signal synthesizer uses the model described in Section III-A. The MATLAB code for this model is available at <http://www.cs.stir.ac.uk/~lss/noisyspikes/index.html>.

The first experiment uses a spike shape (spike 1 of Table I) that could be an extracellular signal recorded by placing an electrode very close to a single target neuron (one dominant spike is present with some neural noise). We synthesized a set of neurophysiological signals, which contains this type of dominant spike with seven other correlated plus 15 uncorrelated neural noise signals. We observe the performance of the new algorithm for this set of signals at eight different SNR levels:

TABLE I
FOUR SPIKES USED TO GENERATE DIFFERENT SYNTHESIZED SIGNAL FOR
ALGORITHM PERFORMANCE EVALUATION

	Spike #1	Spike #2	Spike #3	Spike #4
Spike Shape				
Max Ampl	0.2011	0.2156	0.3356	0.1686
Min Ampl	-0.1083	-0.1966	-0.5704	-0.1997
Dur.	2.6ms	3.4ms	3.6ms	3.2ms

These spikes differ in many ways, e.g., amplitude, phase appearance, and duration.

15, 10, 5, 0, -5, -10, and -15 dB. The number of spikes in each test signal is around 50 (i.e., 10 spikes/s).

We apply the new algorithm (*cob*) to each test signal, thus adjusting the threshold level, as discussed in Section III-C, and determined the average hit rate and precision for each noise level. Table II shows the statistics of the hit rate and precision in each category. Analysis of this experiment shows that the *cob* can detect spikes with very high accuracy from the single spike train signal if the SNR is -5 dB or better. Note that the statistics of both hit rate and precision at SNR 0 dB and above are 100% with 0 standard deviation indicating perfect performance.

Since extracellular signals often contain more than one dominant spike train, we study the performance of this algorithm with more realistic synthesized neurophysiological signals. We generate three sets of signals that differ in the number of dominant spike trains. Each test signal contains spike trains of: 1) spike 1 and spike 2; 2) spike 1, spike 2, and spike 3; or 3) all four spike shapes (see Table I). The firing rate of each spike train is approximately 10 Hz (± 1 Hz), giving altogether (in a 5-s test signal) $50 \times n \pm 5$ spikes, where n is the number of dominant spike trains. The noise in each test signal is generated from 7 correlated and 15 uncorrelated neural signals. As in the previous experiment, we adjust the amplitude of neural noise in each test signal to generate seven new test signals at SNR levels: 15, 10, 5, 0, -5, -10, and -15 dB.

The performance (hit rate and precision) of the *cob* on these signals has been observed by applying the algorithm to each test signal separately. We adjusted the threshold level, as discussed in Section III-C. The hit rate and precision are determined for each test signal by comparing with the respective signal's ground truth. The statistics were calculated as for the single dominant spike train mentioned earlier and are shown in Table II. The results show that the mean hit rate and the precision of the *cob* is above 98% with a low standard deviation (less than 2.5%) when the SNR of the test signal is 0 dB or better: this indicates that the algorithm detects more than 98% of true spikes from a 0 dB signal and with around 2.5% false positives. Further, we can trust this result as the average precision is above 95%.

In Fig. 3, we show two graphs to illustrate the overall performance of the algorithm: Fig. 3(a) shows the hit rate, and Fig. 3(b) shows the precision of the algorithm at different SNRs, while

varying the number of dominant spike trains. From these graphs, we conclude that the *cob* can find spikes at 0 dB SNR when there are either single or multiple dominant spike trains. At least 95% of spikes can be correctly detected (with minimal false positives) by the *cob* if the test signal has SNR 0 dB or better. This result can be achieved from the signal generated with up to four dominant spike trains. The technique may show similar performance for more than four dominant spike trains provided that the shapes of all the dominant spikes (in the frequency domain) are not too dissimilar. In the case of dissimilar spike shapes, the technique may overlook one or more spike trains. In such cases, we suggest reapplication of the technique to the same signal with detected spikes replaced by a constant value.

Neurons emit spikes at different rates. We, therefore, assess the *cob* with synthetic extracellular signals that differ in spike rate. We ran an experiment with five sets of synthesized signals at varying overall spike rates: 15, 30, 45, 60, and 75 Hz (± 1 Hz). Each test signal has three dominant spike trains (with shapes 1-3 from Table I) plus seven correlated and 15 uncorrelated neural noise signals at SNR of 5 and 0 dB. As in the previous experiment, we apply the *cob* to each test signal and adjust the threshold level (as described in Section III-C). We determine hit rate and precision from the (known) ground truth. Statistics of both hit rate and precision have been computed, and are shown in Table III. We note that the performance of the algorithm decreases at high spike rates. The mean hit rate at higher spike rates is 1%-3% below the hit rate at lower spike rates. Consequently, the standard deviation becomes higher at high spike rates (above 2%-4%). A high spike rate at low SNR (about 0 dB) results in a greater chance of corrupting the spike shape and its resultant spectra. This is further discussed in Section VI.

E. CoB Technique With Overlapping Spiking Signals

The extracellular signal at any instant is the sum of all contributing spike trains. As a result, overlapping spikes may occur frequently. When a dominant spike overlaps another more distant neuron's low-amplitude spikes (here considered as noise), a portion of the spike near the baseline may become more corrupted (in % terms) than the peak portion of the spike. A simple threshold technique applied after bandpass filtering is enough to detect spike events from this type of signal. On the other hand, the detection of a dominant spike event becomes difficult when the dominant spikes themselves overlap, or when a correlated spike overlaps a dominant spike. These overlapping spikes often change both the dominant spike's amplitude and shape, sometimes producing novel shapes.

To observe the performance of *cob* with overlapping spikes, we consider a test signal containing two dominant spike trains each firing at around 25 Hz. The spike trains contain spike 1 and spike 2 spike shapes (see Table I). The added neural noise is generated from seven correlated and 15 uncorrelated neurons. The SNR (see Section III-B) of this test signal is 5 dB. A segment of test signal is shown in the top picture of Fig. 4. To demonstrate and analyze the performance of *cob*, we chose two subsegments (shaded areas marked by "A" and "B" in the

TABLE II
PERFORMANCE OF ALGORITHM APPLIED TO SYNTHESIZED NEUROPHYSIOLOGICAL SIGNALS WITH SINGLE, TWO, AND THREE DOMINANT SPIKE TRAINS

		Hit Rate			Precision		
		mean \pm std	min	max	mean \pm std	min	max
Single spike trains	15dB	100 \pm 0	100.00	100.00	100 \pm 0	100.00	100.00
	10dB	100 \pm 0	100.00	100.00	100 \pm 0	100.00	100.00
	5dB	100 \pm 0	100.00	100.00	100 \pm 0	100.00	100.00
	0dB	100 \pm 0	100.00	100.00	100 \pm 0	100.00	100.00
	-5dB	99.8 \pm 0.6	97.87	100.00	99.3 \pm 1.6	91.52	100.00
	-10dB	87.9 \pm 21.9	3.63	100.00	79.3 \pm 13.1	51.76	100.00
	-15dB	9.9 \pm 22.7	0.00	90.19	40.6 \pm 38.2	0.00	100.00
Two spike trains	15dB	99.9 \pm 0.2	98.96	100.00	99.96 \pm 0.19	98.96	100.00
	10dB	99.9 \pm 0.2	98.96	100.00	99.9 \pm 0.2	98.95	100.00
	5dB	99.9 \pm 0.2	98.95	100.00	99.9 \pm 0.3	98.95	100.00
	0dB	99.7 \pm 0.8	95.87	100.00	99.4 \pm 1.3	93.00	100.00
	-5dB	92.7 \pm 13.4	47.05	100.00	89.9 \pm 9.6	66.18	100.00
	-10dB	48.1 \pm 32.9	0.00	100.00	72.2 \pm 24.5	0.00	100.00
	-15dB	7.0 \pm 20.2	0.00	97.91	25.9 \pm 35.2	0.00	100.00
Three spike trains	15dB	99.9 \pm 0.3	98.70	100.00	99.8 \pm 0.4	98.05	100.00
	10dB	99.8 \pm 0.4	98.01	100.00	99.6 \pm 0.6	96.73	100.00
	5dB	99.9 \pm 0.3	99.31	100.00	99.7 \pm 0.6	97.45	100.00
	0dB	98.2 \pm 2.3	87.91	100.00	95.7 \pm 5.9	76.83	100.00
	-5dB	69.8 \pm 27.3	27.39	100.00	79.7 \pm 12.1	57.04	98.11
	-10dB	14.5 \pm 19.5	0.00	66.20	39.9 \pm 37.3	0.00	100.00
	-15dB	0.9 \pm 4.4	0.00	31.03	15.9 \pm 29.7	0.00	100.00

Each Experiment is conducted on one set of signals (50 test signals each with duration of 5 s) at seven different SNR values. Hit rate and precision are computed using (10).

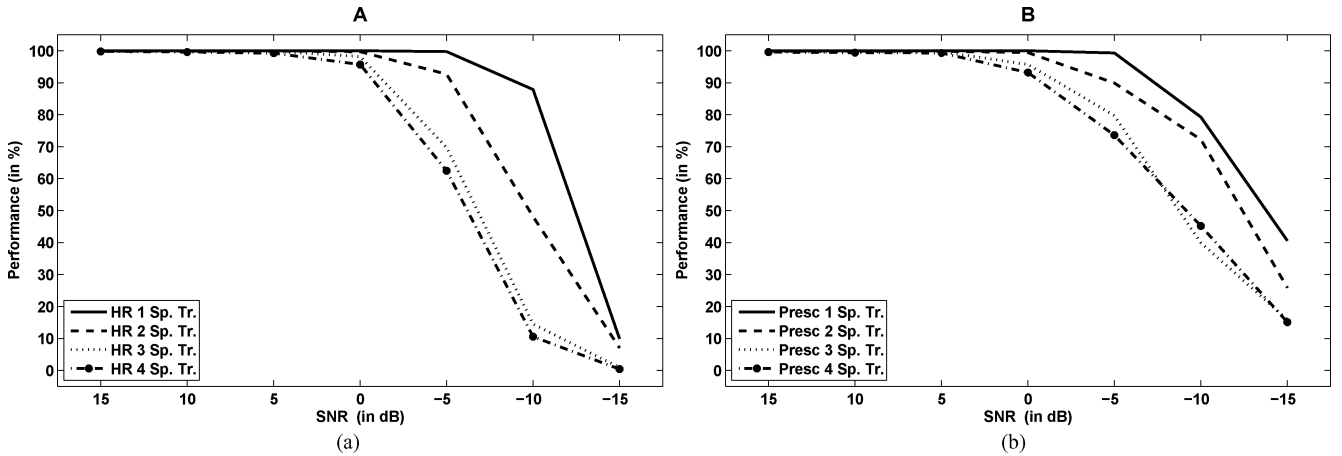


Fig. 3. Overview of the algorithm's performance on synthesized neurophysiological signals. The graphs show (a) the mean hit rate and (b) the mean precision (right) for different sets of signals (each set contains 50 five-second-long test signals) with different numbers of dominant spikes and different SNRs. The spike rate from each dominant spike train in any test signal is 10 spikes/s.

figure). The zoom-in presentation of these subsegment signals is shown in the bottom pictures of Fig. 4. To show the form of the overlapping signal, we also display the dominant spike trains (marked as "a") and the sum of the dominant spike trains (marked as "b") for that particular period of raw signal (marked as "c"). We apply *cob* to the raw signal. The detected spike events (marked as "d") for the respective subsegment signals are shown in the same figure.

As can be seen in the lower figures, spikes from the two dominant spike trains collide (overlap) at "x" and "y." Due to the addition of correlated spikes (plus uncorrelated noise),

the shape of these single dominant spikes has been changed. Sometimes the correlated spike amplitude is higher than the related single dominant spike. However, the *cob* does not detect these as spike. It detects only the dominant spike event.

When two dominant spikes are superimposed, the resultant spike shape changes: in the bottom-right figure, the resultant spike appears as a double-headed single spike (inset), and in the bottom-left figure, the resultant spike is a new spike with a higher amplitude and a longer duration of each phase. In addition, the additive correlated and uncorrelated noise changes the shape of the overlapped resultant spike. Event detection results produced

TABLE III
PERFORMANCE STATISTICS OF ALGORITHM ON FIVE SETS (EACH SET CONTAINS 50 FIVE-SECOND-LONG TEST SIGNALS)
OF SYNTHESIZED NEUROPHYSIOLOGICAL SIGNALS DIFFERING IN SPIKE RATE

SNR	Spike	Hit Rate			Precision		
	Rate	mean \pm std	min	max	mean \pm std	min	max
5dB	15	99.8 \pm 0.5	98.59	100	99.6 \pm 1.6	89.53	100.00
	30	99.8 \pm 0.3	98.63	100	99.8 \pm 0.6	96.64	100.00
	45	99.6 \pm 1.1	92.76	100	99.1 \pm 1.8	88.36	100.00
	60	99.5 \pm 1.2	93.37	100	99.0 \pm 2.2	89.27	100.00
	75	98.9 \pm 1.9	90.13	100	98.4 \pm 1.9	92.07	100.00
0dB	15	99.1 \pm 1.9	91.78	100	98.7 \pm 2.4	91.02	100.00
	30	98.7 \pm 1.6	92.20	100	95.4 \pm 6.8	76.71	100.00
	45	97.7 \pm 2.6	86.78	100	95.7 \pm 5.1	72.69	100.00
	60	96.7 \pm 4.7	68.45	100	93.4 \pm 5.5	76.58	100.00
	75	96.4 \pm 5.9	69.27	100	93.7 \pm 5.3	79.56	99.73

Total spike rates of 15, 30, 45, 60, and 75 Hz were used each test signal has three dominant spike trains with spike rates of 5, 15, 10, 20 and 25 spikes/s. The SNRs are 5 and 0 dB. The statistics of hit rate and precision are computed from 50 similar examples of test signals.

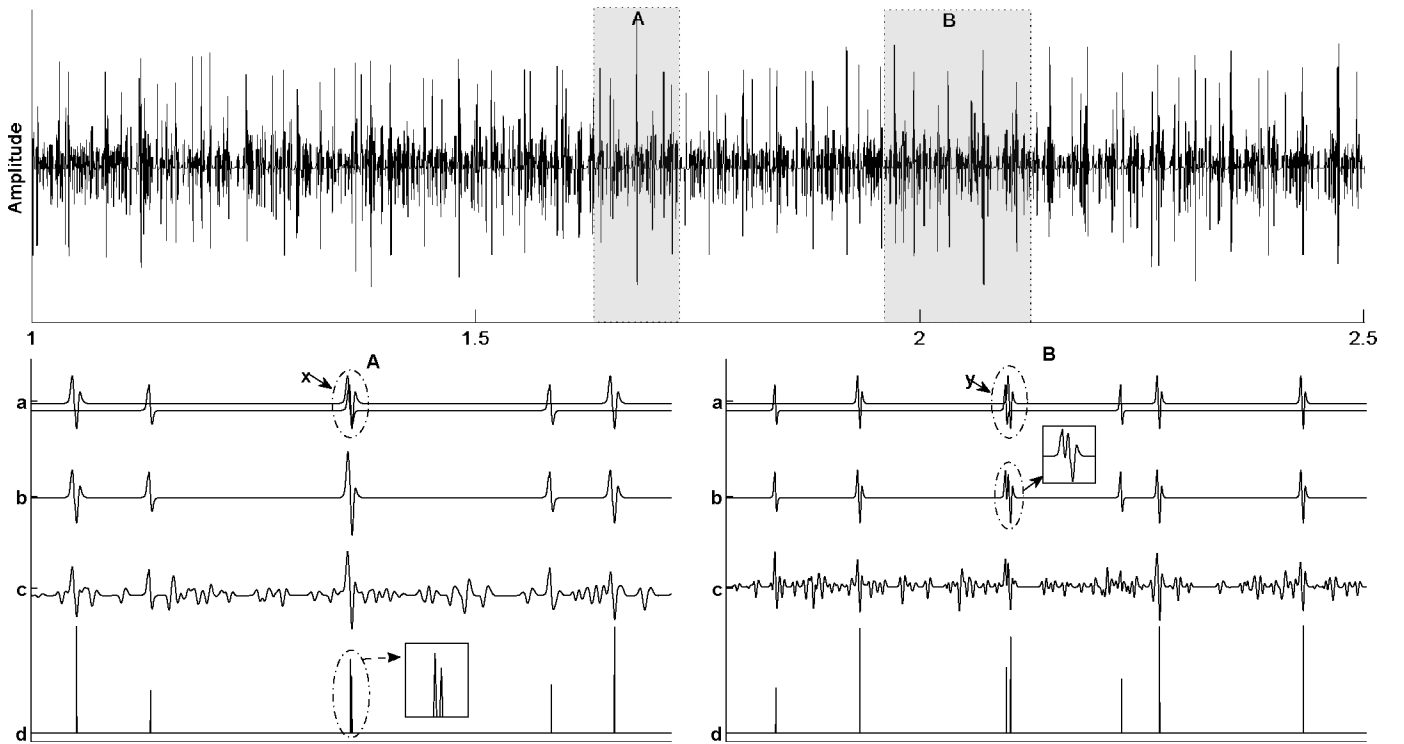


Fig. 4. Performance of *cob* to the overlapping spike signal. Top shows original signal, with parts “A” and “B” shown magnified at waveform “c” in the two lower panels. “a” and “b” in the lower panels show the original spike signals and their sum, and “d” shows the detected spike events. The parts of the signals a marked “x” and “y” show overlapping spike events.

by the *cob* technique show the presence of two spikes resulting from the superimposed spikes. The time duration between the two peak values of these spikes is 0.25 ms for the overlap signal at “x” and 0.75 ms for the overlap signal at “y.”

F. Comparison With Other Techniques

We compare the *cob* with five established spike detection methods. These are a wavelet-based technique (*wav*) [4], a simple double-sided amplitude thresholding technique (*dtl*), a time-windowed doubled-sided amplitude threshold (*pln*) [10],

a morphological filtering-based technique (*mor*) [18], and a NEO-based technique (*neo*) [14]. We programmed the algorithms for the aforementioned techniques, except for *wav*, since its software was provided by Nenadic and Burdick [4]. We tune the key parameters of each algorithm in order to achieve the best possible result. This occurs when the sum of type I (false positive) and type II errors (false negative) is at a minimum. The parameters that we tune are shown in Table IV. Since our test spike train contains spike whose duration (counting all phases) varies from 2 to 3.5 ms, we chose a fixed time window of 3 ms for the technique *pln* and a minimum ISI for all techniques

TABLE IV
PARAMETERS TUNED TO ACHIEVE FOR BEST SPIKE DETECTION FOR EACH
ALGORITHM *cob*, *wav*, *dnl*, *pln*, *mor*, AND *neo*

	Parameter 1	Parameter 2
<i>cob</i>	Threshold amplitude	- -
<i>mor</i>	Structure element size	Threshold Amplitude
<i>wav</i>	Wavelet coeff't no	Wavelet Type
<i>dnl</i>	+ve threshold amplitude	-ve threshold amplitude
<i>pln</i>	+ve threshold amplitude	-ve threshold amplitude
<i>neo</i>	Threshold amplitude	- -

of 3 ms. Spike time estimation is considered correct when the estimate is within 1.5 ms ($0.5 \times$ minimum ISI) of the actual time.

For this experiment, we synthesized a set of signals containing three dominant spike trains, each firing at 10 ± 1 Hz (i.e., a total of about 150 spikes in each 5-s test signal). The noise in each test signal is generated from seven correlated and 15 uncorrelated signals. To observe the algorithms' performance at different noise levels, we adjust the noise level to provide seven SNR levels: 15, 10, 5, 0, -5 , -10 , and -15 dB. We apply all algorithms to all 350 (one set of 50 test signals at seven SNR levels) test signals. The best performance (with appropriate setting of tuning parameters in Table IV) of each algorithm was recorded. We computed the hit rate and precision by comparing detected spike events with the ground truth of each signal. Fig. 5 shows two graphs comparing hit rate and precision at different noise levels for each technique.

The best hit rate is found by *cob* and is more than 99% at SNR 0 dB and better. With the exception of *mor* and *pln*, all other techniques work well when the SNR is 10 dB or higher: We found a hit rate of more than 97% for *wav*, *neo*, *dnl*, and *cob*. The *neo* technique detects around 97% of spike events from the signal at 10 dB SNR, but its precision is not as good (78%). The hit rate for all techniques except *cob* falls gradually with decreasing SNR: at 5 dB SNR, the hit rate is 95%, 89%, and 88%, and at 0 dB, the hit rate is 73%, 51%, and 69% for *dnl*, *wav*, and *neo*, respectively. Similarly, the precision falls with decreasing SNR: at 0 dB, the precision is 72%–75%. *cob* outperforms all other techniques: its hit rate is 99% and 75% at 0 and -5 dB SNR, while the precision values are 97% and 82%, respectively. Note that almost the same performance is observed from *cob* even if the ISI is reduced to 0.5 ms, whereas this is not the case for all the other techniques: their performance deteriorates rapidly as ISI is reduced.

IV. IMPACT OF THRESHOLDING ON *cob*

As can be seen from Fig. 3, the *cob* detects 95% of spikes with around 5% of type I errors (false positives), where the test neurophysiological signal has up to four dominant spikes and the SNR is 0 dB. The detection performance increases when the signal has SNR above 0 dB. But, this accuracy is highly dependent on the setting of the threshold θ_y , i.e., the value of k used in (8).

To demonstrate the effect of the parameter k , we organize another experiment with one set (=50 test signals) of synthe-

sized signals at three different SNR levels. Each test signal is 5 s long and has four dominant spike trains. The spike details are again as in Table I. Each spike train has a spike rate of 10 Hz, so that the overall spike rate is approximately 40 Hz. As in previous experiments, we adjust the level of noise to provide three SNRs: 5, 0, and -5 dB. On each test signal, we apply *cob* at 200 linearly spaced threshold levels by varying k in (8) in linear steps from 0.0025 to 0.9975 (since at zero threshold level, *cob* detects spikes at all points, and at 1, no spikes are detected). The result from each threshold is compared with the ground truth for the respective test signal, and the hit rate and false-positive rate are computed using (10). We determine the mean value of hit rate and the false-positive rate for each SNR, and illustrate the performance of the algorithm using a receiving operating characteristics (ROCs) graph [see Fig. 6(a)].

The ROC curve describes the relationship between the rate of detection of true spike events and the false-positive rate as k is varied (see (8) for k). Clearly, the ROC curve for the signal at 5 dB SNR shows the best detection performance [see zoom-in view of Fig. 6(a)]. Fig. 6(b) shows the hit rate as the threshold k is varied. The data behind the ROC curve for the 5 dB SNR signal show that it is possible to detect 99% of true spike events at 0.14% false-positive rate, i.e., *cob* detects 14 false (extra) events per 10 000 spike detections).

Very similar performance is observed when the test signal has 0 dB SNR. The data for the ROC curve for 0 dB SNR signal show that *cob* can detect a maximum of 99% of true spike events with 2.8% false-positive rate (i.e., 280 false (extra) events per 10 000 spike event detections). Some other data points are: 95% and 90% hit rate at 0.68% and 0.39% false-positive rate, respectively.

The ROC curve for -5 dB SNR signal is different than the other two. Ninety nine percent of true spikes can be detected from this signal with a minimum false-positive rate of 20%. Allowing 12% and 8% false-positive rate, it is possible to detect, respectively, 95% and 90% true spike events.

Clearly, setting the threshold level is a critical task in spike detection using *cob*. Fig. 6(b) illustrates that the hit rate is 1 (i.e., 100% spike detection) when the threshold level is 0 to 0.3 or slightly more. The hit rate falls gradually after that with decreasing threshold level. Therefore, it is difficult to set an appropriate threshold level. A choice of a higher threshold value leads to a low hit rate and low false-positive rate, whereas a choice of lower threshold results in a high hit rate, but at the same time, a high false-positive rate (detecting a large number of false spike events) causing problems at the spike sorting stage. We have seen that the *cob* can detect a higher number of true spike events at a lower false-positive rate for an SNR of 0 dB or better, and is, thus, an improvement over the other techniques. From Fig. 6(b), the best threshold (value for k) was about 0.3–0.35 for SNR of 5 and 0 dB, but 0.2–0.3 for SNR of -5 dB (for the four dominant spike signal). A suitable spike sorting technique must be applied if a lower threshold level is selected because of the increase in false positives. The chosen precise threshold value will also depend on the relative importance of missed spikes and false positives.

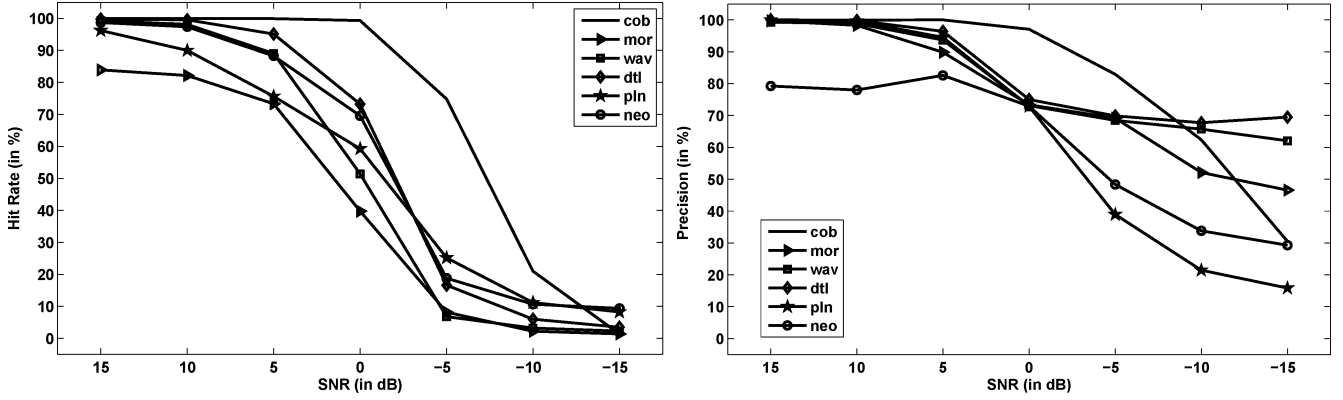


Fig. 5. Comparison of six spike detection techniques: five established techniques and the new technique. The left graph displays the mean hit rate and the right graph displays the mean precision observed. All techniques have been applied to 50 synthesized test signals at seven SNR values: 15, 10, 5, 0, -5, -10, and -15 dB. Each test signals is 5 s long, has three dominant spike trains, and the spike rate is approximately 50 spikes/s.

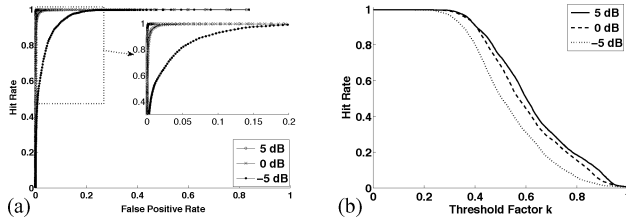


Fig. 6. (a) ROC curve: The performance of the algorithm on the synthesized extracellular signal at three different SNRs: 5, 0, and -5 dB. The test signal has four dominant spike trains each with a spike rate of about 10 Hz. Each ROC curve consists of 200 points, one for each value of k (see (8), where k varies linearly from 0.0025 to 0.9975). Each point plots the hit rate against the false-positive rate for one value of k for each SNR. (b) Hit rate distribution over the threshold factor k [see (8)]. The same three sets of synthesized extracellular signals are used in both figures. The value of k is less critical at 5 dB SNR.

V. SPIKES IN A REAL SIGNAL: APPLYING *cob*

Real biomedical signals always differ from synthetic signals. We, therefore, test our technique on real signals. We observe the performance of the algorithm applied to real signals on two problems: detecting spikes from dendritic recordings, and assessing techniques on data for which simultaneous intracellular and extracellular recordings were available.

We worked with neurophysiological signals recorded from the hippocampus by the Buzsaki Laboratory (<http://osiris.rutgers.edu/>), who have made their data available at <http://crcns.org/data-sets/hc>. We chose this dataset because: 1) it was publicly available and 2) it contains simultaneously recorded intracellular and extracellular data. We first consider an intracellular signal recorded from dendrites. This contains the neuron's internal spike trains plus some other secondary subthreshold intracellular signals. As a result, the intracellular signal appears to have a high noise level. We apply the *cob* to this signal and show the prethreshold output of *cob* in Fig. 7. We high pass (cutoff frequency = 300 Hz) the intracellular signal before processing (and before the illustration). Theoretically, the *cob* without the threshold stage extracts the Dirac delta sequence (from the spikes) plus a lower amplitude noise term [see (2)], and we observe this in Fig. 7. Clearly, the algorithm suppresses the noise and other uncorrelated signals, and at the same time, it highlights

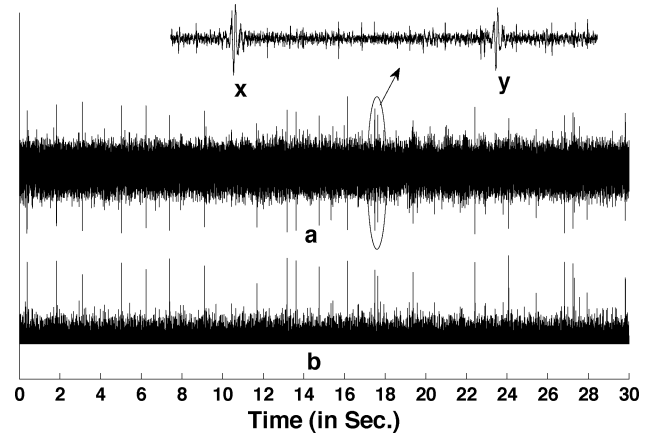


Fig. 7. Application of *cob* to a real signal. (a) Intracellular signal recorded from hippocampus neuron at dendritic location (Buzsaki group: animal: 145, cell: 14921, data file: d14921.001.dat, channel: 5, Segment: 10 to 40 s: the inset shows an expanded version of the circled section showing details of two spikes marked x and y.). (b) *cob*-processed output signal (prior to thresholding). Simple amplitude thresholding can distinguish spike events from subthreshold intracellular noise.

the impulse train. Setting the threshold level for this output signal is now relatively easy, as there is a distinguishable amplitude range between the noise term and the Dirac sequence. Hence, it is possible to detect spike events from this type of noisy signal with very few errors (either false positive or false negative).

To observe the performance of *cob* with a real extracellular signal, we consider three simultaneously recorded (channels) signals from one target neuron: one intracellularly and two extracellularly recorded signals. Our aim is to observe the intracellular spikes in an extracellular signal, and to use this to assess and compare different spike detection techniques. Obviously, the extracellular signal may record more than one spike train, so that we observe spikes from other neurons as well. Fig. 8(a), (b), and (e) illustrate the intracellular and the companion extracellular signals after high-pass filtering with a cutoff frequency of 300 Hz. The extracellular signal of Fig. 8(b) has less noise (we compute the SNR to be around 10 dB); therefore, the spikes are clear, but the other extracellular signal [see Fig. 8(e)] has

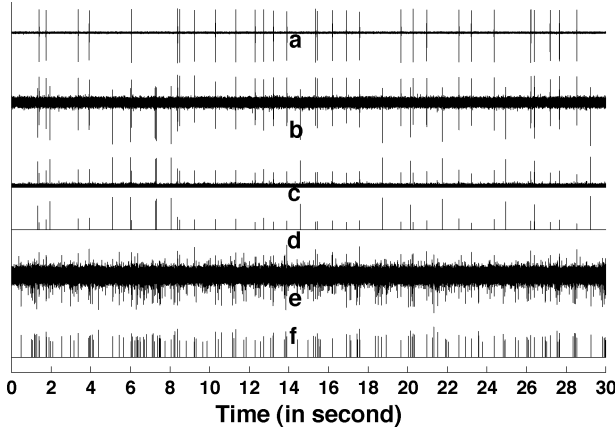


Fig. 8. Application of *cob* to a real signal. (a) Intracellular signal recorded from hippocampus neuron (animal: 166 Cell: 16613 data file: d16613.001.dat, channel: 13, segment: 10 to 40 s). (b) Extracellular signal [channel: 2 recorded simultaneously with intracellular signal at (a)] with electrode placed very close to the target neuron. We calculate the SNR of this signal to be 10.1 dB (c) *cob*-processed and prethresholding output signal. (d) Previous signal with threshold subtracted (threshold factor $k = 0.25$) and negative values set to 0. (e) Extracellular signal [channel: 11 recorded simultaneously with intracellular signal at (a)]. We calculate the SNR to be 3.05 dB and (f) *cob*-processed and thresholded (threshold factor $k = 0.25$) output signal.

more noise (we compute the SNR to be around 3 dB) and also a larger number of different spike shapes from other neurons.

The spikes in the intracellular signal are clear from visual inspection, and we use simple thresholding to identify the spike events in this signal. These spike events are considered as the ground truth for the extracellular signals. The spikes in the extracellular signal “b” are easily identifiable by eye. At least two types of spike are visible in this extracellular signal, and one type matches the intracellular spike train. We apply *cob* to this extracellular signal and show the output before applying a threshold in Fig. 8(c), and after a suitably chosen threshold [threshold factor $k = 0.25$, see (8)] in Fig. 8(d). All visible spikes in the extracellular signal are detected by the *cob* technique. In a similar way, we apply *cob* to the other extracellular signal [see Fig. 8(e)] and apply a threshold to the *cob* processed signal. The thresholded output is illustrated in Fig. 8(f).

Threshold selection is difficult because *cob* detects all spikes regardless of the shape of the spike, or refractory period of spike, i.e., the *cob* technique can detect spikes when the real signal has multiple spike trains. In the signal at “c,” threshold setting is relatively easy. On the other hand, selecting the threshold level for the *cob* processed “e” signal was comparatively hard since the signal has many spike trains and poor SNR. We chose the threshold factor $k = 0.25$ that gives us around 98% hit rate.

To compare the techniques used in Section III-F on this extracellular signal, we adjust the tuning parameters (noted in Table IV) of the respective techniques so that the maximum number of (correctly detected) intracellular spikes (true positive) are matched to minimum number of relative false positives (false only relative to the ground truth provided by the intracellular spike train). The results in Table V were generated by first setting the threshold to the lowest possible value and noting the number of true positives. The threshold was then gradually

TABLE V
RESULT OF APPLYING ALL SIX TECHNIQUES TO EXTRACELLULAR DATA, USING INTRACELLULAR EVENTS AS GROUND TRUTH

Δt ms			<i>cob</i>	<i>wav</i>	<i>mor</i>	<i>dlt</i>	<i>pln</i>	<i>neo</i>
Ch 2 Sig ‘b’	0.5	TP	30	16	29	30	29	30
		FN	0	14	1	0	1	0
		RFP	15	29	16	16	1	139
	1.0	TP	30	30	30	30	30	30
		FN	0	0	0	0	0	0
		RFP	14	14	14	15	0	112
Ch 11 Sig ‘e’	0.5	TP	30	26	9	27	17	30
		FN	0	4	21	3	13	0
		RFP	106	123	71	113	24	4099
	1.0	TP	30	28	27	30	30	30
		FN	0	2	3	0	0	0
		RFP	106	33	91	58	18	178

Δt shows the maximum permitted interval between a detected spike and a spike in the ground truth. TP = true positive, FN = false negative, and RFP = relative false positive.

increased until just before the point at which the number of true positives started to drop. The results were then recorded. Table V shows results from all six techniques. Since the extracellular signal has spikes from multiple neurons and all our observations were relative to the intracellular spike train, the spikes from other neurons are termed here as relative false positives. The accuracy with which a spike needs to be found (Δt in Table V) makes a considerable difference to the results (note that Δt is also the minimum ISI findable using any of the techniques).

For signal “b” at $\Delta t = 0.5$ ms, *cob*, *dlt*, and *neo* find all the intracellular spikes. *pln* and *mor* miss one spike, but *wav* misses many of them. However, all the techniques find all the intracellular spikes [i.e., 0 false negative (or missing)] when $\Delta t = 1$ ms. On the other hand, when the extracellular signal has a lower SNR and a higher number of spikes (signal “e”), the techniques *cob* and *neo* work best at $\Delta t = 0.5$ ms, followed by *wav* and *dlt*. *neo* is capable of detecting all true positives, but at the cost of large numbers of relative false positives: if we permit it to miss some spikes, the number of relative false positives falls rapidly. Though *pln* detects 50% of intercellular spikes when $\Delta t = 0.5$ ms, the *mor* almost fails to detect intracellular spike events. At $\Delta t = 1$ ms, *cob*, *neo*, *dlt*, and *pln* successfully detect all intracellular spike events from signal “e,” and the others only miss a small number.

It is observed that at lower Δt , *dlt* and *pln* sometimes detect a multipolar spike as a number of nearby neurons’ spikes. But, when Δt is increased, detected spikes that are closer together are no longer classified as different spikes. In addition, *pln* includes an allowance for the refractory period, reducing the number of relative false positives found. This is useful when there is known to be a single dominant spike train, but could result in missed spikes when there is more than one dominant spike train. The reason for *wav* misclassifying many of the intracellular spikes when $\Delta t = 0.5$ ms is that the time of the spike is inaccurately estimated; hence, when $\Delta t = 1$ ms, *wav* performs much better. Overall, we conclude that *cob* produces more accurately timed estimates, and does not get confused by multipolar extracellular signals, refractory periods, or minimum ISIs.

VI. DISCUSSION AND CONCLUSION

The key idea of this new technique is signal deconvolution using an adaptive inverse filter. Estimation of the inverse filter is based on the *cob* and this needs a sufficiently large volume of data. Thus, for example, in Table III, when the spike rate is 5 Hz, it sometimes fails to find one spike type. The amount of data to be processed at a time can be extended (or reduced) depending on the signal of interest and the frequency of its occurrence, e.g., to observe spikes from within the delta band of an EEG signal, a considerably longer duration would need to be processed. Note that a very long dataset may violate the stationarity and linearity conditions for bispectrum estimation [39].

The new technique is essentially independent of sampling frequency. The number of points used in FFT estimation (converting the signal from the time domain to frequency domain) should be equivalent to at least double the duration of a spike shape: here, we have used 256 samples throughout, equivalent to 12.8 ms.

The critical step in this technique is the estimation of the inverse filter. From previous work [30], *cob* can reconstruct any filter (minimum, nonminimum, or maximum phase system) information with very low variance from any Poisson triggered (non-Gaussian) (LTI) filtered process. Further, *cob* can reconstruct the filter from the signal at very low SNR. Hence, we apply the *cob*-based reconstructed filter to the signal for inverse filtering, so that we can find the trigger sequence. We observe in all experiments with synthetic signals that the trigger sequence has been estimated from the signal at 0 dB SNR or below, and this has been possible due to the properties of *cob*. In the experiments on real data, we used high-pass (300 Hz) filtered data for testing all the techniques. Clearly, high-pass filtering is critical for *pln* and *dlt*; however, *cob* will, in fact, work on raw data, primarily because it works in the frequency domain.

Unlike any fixed wavelet-based signal processing, *cob* uses an adaptive inverse filter to perform the deconvolution. If an inverse filter is estimated accurately, *cob* can detect nearly 100% of spike events. This inverse filter information is estimated from the signal in which the spike is detected. Therefore, theoretically, there must have been spikes in the signal. Again, if there is one dominant spike train in the signal, it is observed that *cob* can estimate the inverse filter from the signal at low spike firing rate (<5 Hz). But, if the signal has more than one dominant spike train, an average inverse filter is estimated. The averaging is dependent on the spike trains in the signal, i.e., the rate of spikes in each spike train, frequency components of the spike, etc. We observed that sometimes *cob* fails to detect one spike train in an extracellular signal that contains multiple dominant spike trains. This happens when one spike train has a much lower spike rate than the other spike trains. This is, in fact, a failure of accurate inverse filter estimation. We suggest considering a longer signal or a lower resolution of the frequency domain components. We are also considering iterative application of the *cob* technique, ignoring spikes already found in the next application. In addition, choosing the threshold level may be difficult if the signal has many completely superimposed spike events: this can impair detecting other spike events.

One clear advantage of this algorithm is higher precision compared to other techniques. With the appropriate threshold, *cob* has few or no false positives. We found that the established techniques almost fail to detect spikes (low hit rate) when the test signal's SNR is 0 dB or even better, whereas the *cob* detects almost all (hit rate is very high). The method *pln* detects events without preprocessing, and as a result, it is subject to false-positive and/or false-negative errors. The technique *mor* suppresses noise on the basis of the shape of the spike signal and noise. However, it can fail to detect spike events if a spike signal is corrupted by noise and changes its shape. Some noise shapes can be interpreted as false spikes. The technique *wav* uses a wavelet transformation and its coefficients. The choice of mother wavelet is crucial because the spike shapes may differ considerably and because spikes are corrupted in different ways by noise. Thus, *wav* fails to detect some spike signals and can give errors even at high SNR (see Fig. 5). The technique *neo* provides the instantaneous nonlinear energy without checking the spike shape, and therefore, tends to false-positive errors. The method *cob* uses a more sophisticated preprocessing technique that inverts the original convolution caused by the geometry of the target neuron and the electrode. This makes it much more immune to additive noise. This matters because many electrophysiological signals have poor SNR. We note that it assumes a single convolution for all the target neurons, which is not likely to be the case. However, the time-domain statistics of the different convolutions are likely to be similar, if only, because the original intracellular signals are similar.

Detecting spike events in an extracellular neurophysiological signal is a challenge in two particular cases: where there is no prior information about the number of spike trains or the number of spikes per second and where the noise level is high. It is always possible that some spikes appear with low amplitude due to interaction with additive noise. As a result, as seen in Section V, different spike detection methods applied to a real signal do not always locate the same events. Reducing the threshold level for all methods may locate more possible events, but at the expense of increasing the number of inserted events. When *cob* is applied to a synthesized signal, it generates relatively few errors caused by false positives (even in poor SNR), suggesting that we can rely on its detected events more than with other techniques.

Finally, the MATLAB code and some simulated data used in this paper are available at Web page: <http://www.cs.stir.ac.uk/~ssh/spikedetection>.

ACKNOWLEDGMENT

The authors would like to thank the anonymous referees for useful comments that have assisted them in greatly improving upon an earlier draft.

REFERENCES

- [1] L. S. Smith and N. Mtetwa, "A tool for synthesizing spike trains with realistic interference," *J. Neurosci. Methods*, vol. 159, no. 1, pp. 170–180, 2007.
- [2] G. R. Holt and C. Koch, "Electrical interactions via the extracellular potential near cell bodies," *J. Comput. Neurosci.*, vol. 6, no. 2, pp. 169–184, 1999.

- [3] R. Chandra and L. Optican, "Detection, classification, and superposition resolution of action potentials in multiunit single-channel recordings by an on-line real-time neural network," *IEEE Trans. Biomed. Eng.*, vol. 44, no. 5, pp. 403–412, May 1997.
- [4] Z. Nenadic and J. Burdick, "Spike detection using continuous wavelet transform," *IEEE Trans. Biomed. Eng.*, vol. 52, no. 1, pp. 74–87, Jan. 2005.
- [5] S. Bierer and D. Anderson, "Multichannel spike detection and sorting using an array processing technique," *Neurocomputing*, vol. 26/27, pp. 947–956, 1999.
- [6] E. M. Schmidt, "Computer separation of multi-unit neuroelectric data: A review," *J. Neurosci. Methods*, vol. 12, no. 2, pp. 95–111, 1984.
- [7] H. Bergman and M. DeLong, "A personal computer-based spike detector and sorter: Implementation and evaluation," *J. Neurosci. Methods*, vol. 41, pp. 187–197, 1992.
- [8] R. Harrison, "A low-power integrated circuit for adaptive detection of action potentials in noisy signals," in *Proc. Int. Conf. IEEE EMBC*, 2003, vol. 4, pp. 3325–3328.
- [9] L. Smith, S. Shahid, A. Vernier, and N. Mtetwa, "Finding events in noisy signals," in *Proc. Irish Signals Syst. Conf.*, 2007, pp. 31–35.
- [10] T. Borghi, R. Gusmerol, A. S. Spinelli, and G. Baranauskas, "A simple method for efficient spike detection in multiunit recordings," *J. Neurosci. Methods*, vol. 163, no. 1, pp. 176–180, 2007.
- [11] I. Obeid and P. Wolf, "Evaluation of spike detection algorithms for a brain-machine interface application," *IEEE Trans. Biomed. Eng.*, vol. 51, no. 6, pp. 905–911, Jun. 2004.
- [12] A. F. Atiya, "Recognition of multiunit neural signals," *IEEE Trans. Biomed. Eng.*, vol. 39, no. 7, pp. 723–729, Jul. 1992.
- [13] J. Kaiser, "On a simple algorithm to calculate the 'energy' of a signal," in *Proc. Int. Conf. IEEE ASSP*, 1990, vol. 1, pp. 381–384.
- [14] K. Kim and S. Kim, "Neural spike sorting under nearly 0-db signal-to-noise ratio using nonlinear energy operator and artificial neural-network classifier," *IEEE Trans. Biomed. Eng.*, vol. 47, no. 10, pp. 1406–1411, Oct. 2000.
- [15] P. Maragos, J. Kaiser, and T. F. Quatieri, "On amplitude and frequency demodulation using energy operators," *IEEE Trans. Signal Process.*, vol. 41, no. 4, pp. 1532–1550, Apr. 1993.
- [16] S. Mukhopadhyay and G. Ray, "A new interpretation of the nonlinear energy operator and its efficacy in spike detection," *IEEE Trans. Biomed. Eng.*, vol. 45, no. 2, pp. 180–187, Feb. 1998.
- [17] P. García, C. P. Suárez, J. Rodríguez, and M. Rodríguez, "Unsupervised classification of neural spikes with a hybrid multilayer artificial neural network," *J. Neurosci. Methods*, vol. 82, no. 1, pp. 59–73, 1998.
- [18] G. Xu, J. Wang, Q. Zhang, S. Zhang, and J. Zhu, "A spike detection method in EEG based on improved morphological filter," *Comput. Biol. Med.*, vol. 37, no. 11, pp. 1647–1652, 2007.
- [19] R. Gonzalez and P. Wintz, *Digital Image Processing*, 2nd ed. Reading, MA: Addison-Wesley, 1987.
- [20] A. Abeles and M. Goldstein, "Multispike train analysis," *Proc. IEEE*, vol. 65, no. 5, pp. 762–773, May 1977.
- [21] E. Goodall and K. Horch, "Separation of action potentials in multiunit intrafascicular recordings," *IEEE Trans. Biomed. Eng.*, vol. 39, no. 3, pp. 289–295, Mar. 1992.
- [22] C. Olson, "Maximum-likelihood template matching," in *Proc. IEEE Comput. Soc. Conf. Comput. Vis. Pattern Recognit.*, 2000, pp. 52–57.
- [23] N. Mtetwa and L. S. Smith, "Smoothing and thresholding in neuronal spike detection," *Neurocomputing*, vol. 69, no. 10–12, pp. 1366–1370, 2006.
- [24] H. Kaneko, S. Suzuki, J. Okada, and M. Akamatsu, "Multineuronal spike classification based on multisite electrode recording, whole-waveform analysis, and hierarchical clustering," *IEEE Trans. Biomed. Eng.*, vol. 46, no. 3, pp. 280–290, Mar. 1999.
- [25] C. Olson, "Maximum-likelihood image matching," *IEEE Trans. Pattern Anal. Mach. Intell.*, vol. 24, no. 6, pp. 853–857, Jun. 2002.
- [26] X. Yang and S. Shamma, "A totally automated system for the detection and classification of neural spikes," *IEEE Trans. Biomed. Eng.*, vol. BME-35, no. 10, pp. 806–816, Oct. 1988.
- [27] G. Zouridakis and D. Tam, "Multi-unit spike discrimination using wavelet transforms," *Comput. Biol. Med.*, vol. 27, pp. 9–18, 1997.
- [28] J. Letelier and P. Wever, "Spike sorting based on discrete wavelet transform coefficients," *J. Neurosci. Methods*, vol. 101, no. 2, pp. 93–106, 2000.
- [29] K. Kim and S. Kim, "A wavelet-based method for action potential detection from extracellular neural signal recording with low signal-to-noise ratio," *IEEE Trans. Biomed. Eng.*, vol. 50, no. 8, pp. 999–1011, Aug. 2003.
- [30] S. Shahid and J. Walker, "Cepstrum of bispectrum—A new approach to blind system reconstruction," *Signal Process.*, vol. 88, no. 1, pp. 19–32, 2008.
- [31] S. Shahid and L. S. Smith, "A novel technique for spike detection in extracellular neurophysiological recordings using cepstrum of bispectrum," in *Proc. Eur. Signal Process. Conf.*, 2008, pp. 19–32.
- [32] D. Henze, Z. Borhegyi, J. Csicsvari, A. Mamiya, K. Harris, and G. Buzsaki, "Intracellular features predicted by extracellular recordings in the hippocampus in vivo," *J. Neurophysiol.*, vol. 84, pp. 390–400, 2000.
- [33] S. Shahid, J. Walker, G. Lyons, C. Byrne, and A. Nene, "Application of higher order statistics techniques to EMG signals to characterize the motor unit action potential," *IEEE Trans. Biomed. Eng.*, vol. 52, no. 7, pp. 1195–1209, Jul. 2005.
- [34] A. Papoulis and A. Pillai, *Probability, Random Variables and Stochastic Processes*, 4th ed. New York: McGraw-Hill, 2002.
- [35] C. Nikias and M. Raghuveer, "Bispectrum estimation: A digital signal processing framework," *Proc. IEEE*, vol. 75, no. 7, pp. 869–891, Jul. 1987.
- [36] *Wavelet Toolbox User's Guide*. The MathWorks, Inc., Natick, MA, Version 3, 2006.
- [37] R. Quiroga, Z. Nadasdy, and Y. Ben-Shaul, "Unsupervised spike detection and sorting with wavelets and superparamagnetic clustering," *Neural Comput.*, vol. 16, pp. 1661–1687, 2004.
- [38] T. Fawcett, "An introduction to ROC analysis," *Pattern Recognit. Lett.*, vol. 27, no. 8, pp. 861–874, 2006.
- [39] C. Nikias and J. Mendel, "Signal processing with higher-order spectra," *IEEE Signal. Proc. Mag.*, vol. 10, no. 3, pp. 10–37, Jul. 1993.



Shahjahan Shahid was born in Bogra, Bangladesh, on March 1964. He received the B.Sc. and M.Sc. degrees in applied physics and electronics from the University of Rajshahi, Rajshahi, Bangladesh, in 1988 and 1990, respectively, and the Ph.D. degree in electronics and computer engineering from the University of Limerick, Limerick, Ireland, in 2004.

From 1991 to 1997, he was with the Bangladesh Atomic Energy Commission as a Scientific Officer. From 2004 to 2006, he was with Guger Technologies, Graz, Austria. In 2007, he joined the University of Stirling, Stirling, U.K. He is currently with the University of Ulster, Coleraine, U.K. His research interests include higher order statistical signal processing and its applications in estimation theory, biosignal analysis, neural spike detection, and brain-computer interfacing.



Jacqueline Walker (M'90) was born in London, U.K. She received the B.A. and B.E. (First Class Honors) degrees from the University of Western Australia, Perth, W.A., Australia, in 1988 and 1993, respectively, and the Ph.D. degree from Curtin University of Technology, Perth, in 1997.

From 1996 to 1997, she was a Research Engineer in the Australian Telecommunications Research Institute. In November 1997, she joined the Department of Electronic and Computer Engineering, University of Limerick, Limerick, Ireland, as a Lecturer. Her research interests include signal processing applied to biomedical, speech and music signals with particular interest in blind deconvolution and blind source separation.

Dr Walker is a Member of the Institute of Electrical Engineers.



Leslie S. Smith (M'85–SM'04) received the B.Sc. and Ph.D. degrees from Glasgow University, Glasgow, U.K., in 1973 and 1981, respectively.

He was in industry. He was a Lecturer at Glasgow University. In 1984, he joined Stirling University, Stirling, U.K., where he is currently a Professor and the Head of the Department. His research interests include neural systems, both from a computational modeling and a neuroinformatics viewpoint.

Prof. Smith is a member of the Society for Neurosciences and the American Society of Acoustics.